To cite this article: ZONG Z, CHEN Z Y. Ship resistance in random ice field of small ice floes made of the substitute material[J/OL]. Chinese Journal of Ship Research, 2022, 17(5). http://www.ship-research.com/en/article/doi/10.19693/j.issn.1673-3185.02847.

DOI: 10.19693/j.issn.1673-3185. 02847

Ship resistance in random ice field of brash ice made of the substitute material

ZONG Zhi[*1,2], *CHEN Zhaoyang*[1]

1 School of Naval Architecture & Ocean Engineering, Dalian University of Technology, Dalian 116024, China

2 State Key Laboratory of Structural Analysis for Industrial Equipment, Dalian 116024, China

Abstract: [**Objectives**] This study focuses on the feasibility of a ship resistance model test in an ice field of small ice floes made of substitute material in order to reveal the resistance components and thereby provide technical support for the design of ice-going ships. [**Methods**] Ship resistance test in ice floes made of polypropylene (PP) instead of natural refrigerated ice is conducted. By adjusting the sizes, shapes, numbers of ice floes, the random ice field with a given concentration is generated. The geometric phase transition theory predicts that there exists a critical concentration which divides the random ice field into discrete phase (concentration is less than critical value) and connected phase (concentration is greater than critical value).[**Results**] The main components of ice resistance in the discrete phase are open water resistance and ship-ice collision resistance, while ice resistance in the connected phase includes ice friction resistance, open water friction resistance and collision resistance. If the fractal dimension of the random ice field is used to redefine the ice resistance coefficient, it is nearly constant in the trial range (speed 0.3−0.9 m/s) when the concentration is smaller than the critical value. When the concentration is greater than the critical value, the ice friction resistance is inversely proportional to speed. [**Conclusions**] Polypropylene can replace frozen ice in the prediction of ice resistance. The pure ice resistance of an ice field is divided into two components: ice resistance arising from collision and ice friction resistance arising from accumulation.

Key words: brash ice; resistance; collision; friction

CLC number: U661.31^{+}1

0 Introduction

In recent years, the melting of the Arctic ice has led to a surge in the demand for Arctic shipping. The volume of freight on the Arctic routes increased from 3.9×10^4 t to 1.28×10^6 t from 2015 to 2020, and it was expected to reach 9×10^7 t in 2030 and 1.3×10^8 t in 2035 [1-2]. Moreover, the melting of the ice has also promoted the exploitation of Arctic resources. The Yamal LNG Plant, located in Sabbetta in the Arctic Ocean, was put into production in 2019, with an annual production capacity of 1.65×10^7 t. Its liquefied natural gas (LNG) has been exported to Asia by ice-going ships [3].

The Arctic ice surface and the route behind an icebreaker are often covered with brash ice even in summer. As a result, polar ships sail among brash ice most of the time. Therefore, studying the resistance on ships in brash ice (here, it refers to small ice blocks at a scale smaller than that of ships) helps to evaluate the performance of ships sailing in polar regions accurately. For this reason, it has become a research topic of great concern in recent years [4-8].

To verify the numerical method for predicting resistance in brash ice, MARIN started to investigate the feasibility of using artificial brash ice (non-frozen ice) made of polypropylene instead of natural low-temperature frozen ice for the model test in 2013 [4-5]. The artificial brash ice is controllable: Re-

Received: 2022 − 04 − 13 **Accepted:** 2022 − 07 − 14

Supported by: National Natural Science Foundation of China (52192692, 52171294)

Authors: ZONG Zhi, male, born in 1964, Ph.D., professor. Research interest: hydrodynamics, high-performance ships, and ship-ice-water dynamics. E-mail: zongzhi@dlut.edu.cn

CHEN Zhaoyang, male, born in 1995, master degree candidate. Research interest: ship-ice-water dynamics

***Corresponding author:** ZONG Zhi

searchers can set the same initial conditions (such as ice thickness, size, and density) as those in the numerical model and the same mechanical model (such as rigid brash ice blocks). Hence, the numerical model and model test can be directly compared and verified more easily.

Recent research has revealed many new phenomena. For example, Guo et al. [6] observed special speed points on the speed curve, concluding that they were spawned by instability. Zong et al. [7] found the "hull-fitting" phenomenon in the model test, predicted that the phenomenon could also be observed in a full-scale ship by scale conversion, and provided a video of a full-scale ship test. Zuev et al.[8] obtained an empirical formula for resistance prediction through alternative tests. In particular, the influence of concentration is empirically expressed as the square of a sine function. Yet, these studies fail to provide a robust and systematic ice resistance mechanism and prediction method.

This paper further explored the feasibility of a resistance model test in brash ice made of polypropylene instead of natural frozen ice, especially the preparation of a brash ice field. The components and change law of brash ice resistance were also investigated to provide technical support for the design of ships sailing in brash ice regions.

1 Test setup

In this paper, the resistance test of a ship sailing in a brash ice region was carried out in the towing tank of the Dalian University of Technology. The tank is 160 m×7.0 m×4.0 m in size; the trailer, equipped with a four-degree-of-freedom seaworthiness instrument, has a minimum speed of 0.1 m/s and a maximum speed of 8.0 m/s. The total resistance on the ship model is measured by a resistance sensor. The relevant test data are collected by a test data acquisition system with a signal acquisition frequency of 50 Hz. The sensor range is 30 kgf, and the sensor accuracy is 0.1% of the maximum range.

1.1 Ship model

The test used a model of an ice-going LNG that mainly sailed in sea routes with brash ice and routes opened by icebreakers. The principal dimensions of the full-scale ship and the ship model are shown in Table 1. The scale ratio is 50∶1.

1.2 Preparation of brash ice field

The largest difference between a brash ice field and layered ice is that the former is a random field composed of ice blocks with different sizes and shapes, as shown in Fig. 1. The model test should provide a similar random ice field, as illustrated in Fig. 2. From the perspective of similarity, building such a random ice field should highlight at least the following five factors:

Table 1 Principal dimensions of full-scale ship and ship model

Principal dimension	Full-scale ship	Model
Total length/m	218.13	4.36
Waterline length/m	210	4.2
Molded breadth/m	32.8	0.656
Molded depth/m	18.2	0.364
Wetted surface area/m^2	9 380.60	3.75
Displacement/t	50 450	0.394

1) Concentration.

Concentration is the percentage of ice on the water surface per unit area, expressed by ϕ. ϕ=0 means open water without ice; ϕ = 1 indicates a water area completely covered by ice (the connected phase). When ϕ is within 0−1, a critical concentration $0 < \phi_c \leqslant 1$ exists. When $\phi < \phi_c$, almost all brash ice blocks are discrete. This case is called the discrete phase, and no contact among brash ice blocks is assumed, as shown in Fig. 3(a). When the concentration changes continuously from $\phi < \phi_c$ to ϕ_c, the discrete phase composed of non-contact ice blocks in the ice field suddenly undergoes the geometric phase transition into a connected phase (as shown by the red ice blocks in Fig. 3(b)). A continuous chain exists in the connected phase, and each brash ice block in the

Fig. 1 Xue Long and Xue Long 2 in brash ice

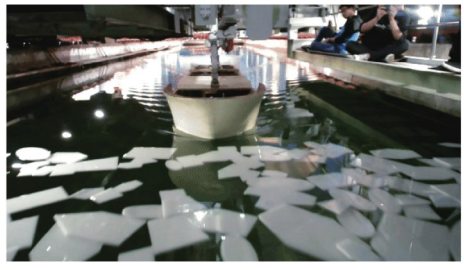

Fig. 2 Ship model in artificial brash ice field

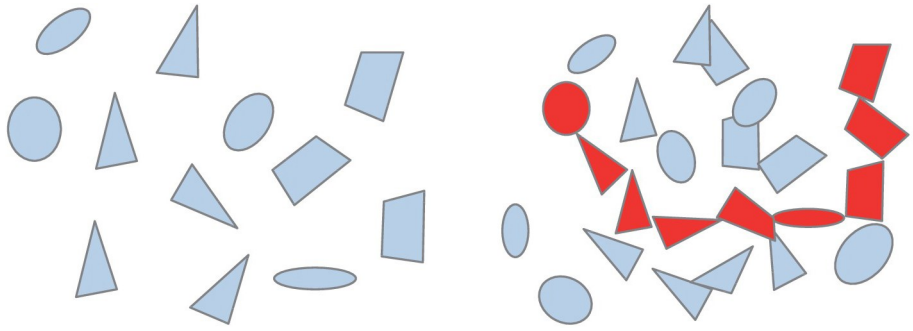

(a) Discrete phase ($\phi < \phi_c$) (b) Connected phase ($\phi < \phi_c$)

Fig. 3 Geometric phase transition near the critical concentration

chain is at least in contact with the other brash ice blocks in the chain, and vice versa. This is an interesting phenomenon of geometric phase transition and falls within the research of "percolation theory" in statistical physics [9-10]. The critical concentration depends on the shape and arrangement of the brash ice blocks. For two-dimensional random shapes and arrangements, an inequality [10] $0.5 < \phi_c < 0.6$ holds. It is a common phenomenon independent of the specific environment.

In this test, the concentration was controlled by changing the number of brash ice blocks in the ice field, and the ice fields with 40%, 50%, 60%, and 70% concentrations were built, respectively.

2) Density of brash ice.

Brash ice blocks are mainly in rigid-body motion if their damage degree is not considered. Therefore, materials with a density similar to that of ice can be used as candidates for artificial brash ice. As the most common materials, polyethylene (PE), polypropylene (PP), and paraffin wax have a density of 0.93, 0.9−0.92, and 0.9−0.91 kg/m^3, respectively, which are close to the ice density 0.917 kg/m^3. PP board was selected for the test in this paper.

3) Feature dimension of brash ice.

In the test, each brash ice block was taken as a whole, regardless of its damage degree. According to elastic mechanics, the feature dimension of a flat plate without damage is [11]

$$d = \sqrt[4]{\frac{D}{k}} \tag{1}$$

where $D = \dfrac{Eh^3}{12(1-\nu^2)}$; $k = \rho_w g$. In the equation, E is Young's modulus; h is ice thickness; ν is Poisson's ratio; ρ_w is the density of water; g is the gravitational acceleration. When the feature dimension of brash ice is smaller than this value, the damage and fracture of brash ice itself can be considered of secondary interest.

According to Eq. (1), the maximum feature dimension of brash ice is 30−40 cm if the ice thickness is set to 2.0−2.5 cm, Young's modulus E is set to 5×10^8 Pa, and Poisson's ratio ν is set to 0.3 in the model test.

4) Characteristic shape of brash ice.

brash ice varies in shape and is thus difficult to prepare one by one in the test. Nevertheless, common geometric shapes can be divided into polygons and ellipses (including circles). For this reason, the following six typical shapes were investigated: rectangle, ellipse, flat trapezoid, slender trapezoid, pentagon, and hexagon. In addition, adjustments were made to each shape under comprehensive consideration (Fig. 4). The maximum sizes were marked in the figure, and various shapes and numbers of brash ice blocks were obtained according to the concentration (Table 2).

5) Distribution pattern of feature dimension of brash ice.

The field measurement in the Arctic shows that the feature dimension of brash ice obeys the power-law distribution [12]. The cumulative quantity distribution $N(d)$ represents the number of brash ice with a feature dimension not smaller than d per unit area presumptively. Then, the distribution of the feature dimension can generally be described by the power law:

$$N(d) = \beta d^{-\alpha} \tag{2}$$

where β is the constant of proportionality, which is different when measured in different sea areas and can thus be measured in the field; α is called fractal dimension[12], indicating the complexity of the distribution of brash ice. When α is one, brash ice is in a straight line; when it is two, brash ice just fills the whole water surface; when it is between one and two, the water surface is partially filled with brash ice. An α closer to two indicates a more complex distribution of brash ice on the water surface [13-14]. brash ice of 1−40 cm has a fractal dimension α of

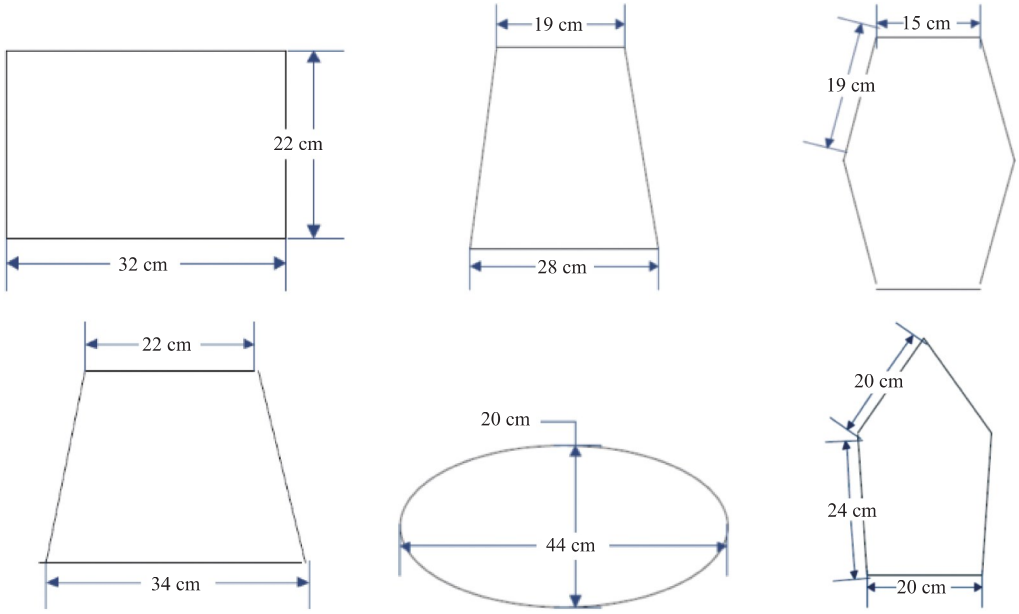

Fig. 4 Six shapes of brash ice blocks prepared in the test (the dimensions in the figure represent maximum values)

Table 2 Dimensions and numbers of ice blocks of six shapes

Rectangle			Flat trapezoid				Slender trapezoid					Pentagon(two upper sides+bottom side+ two lower leg sides)			Hexagon(upper and lower sides+four leg sides)			Ellipse		
Length /cm	Width /cm	Number	Upper base/cm	Lower base/cm	Leg length /cm	Number	Upper base/cm	Lower base/cm	Leg length /cm	Height /cm	Number	Short-side length/ cm	Long-side length/ cm	Number	Short-side length/ cm	Long-side length/ cm	Number	Short-side length/ cm	Long-side length/ cm	Number
32	22	72	22	34.4	26	33	19	27.7	30.4	30.1	34	20	24	66	14.7	18.7	66	20.3	44.3	98
27	18	108	19	29	21	48	16	23	25.3	25.1	48	16.6	20	95	12.3	15.6	99	17	37	95
22	14	149	15	23	17	84	13	18.4	20.2	20.1	84	13.2	16.3	148	9.8	12.5	154	14	30	151
16	11	260	11	17	13	132	9.7	13.8	15.2	15	136	10	12	258	7.4	9.3	259	10	22	254
11	7	553	7	11.5	9	281	6.5	9.2	10	10	276	6.6	8.1	540	5	6.2	535	7	15	550

1.15 [12], which means that the brash ice is spatially distributed in a curve to a small extent. This value may be different in different waters. The spatially fractal distribution is a universally recognized feature of brash ice[12-14].

To build an ice field similar to an actual one, this paper should ensure that the concentration, density, feature dimension, and fractal dimension α of the brash ice in the two ice fields are as same as possible. In addition, the shapes of the brash ice should also be as similar as possible. Therefore, artificial brash ice blocks (left in Fig. 5) and a random ice field they constitute (right in Fig. 5) were prepared for the test.

Fig. 5 Brash ice blocks (left) and corresponding random ice field (right)

1.3 Test scheme and process

Specifically, the floating and load conditions of the ship model were adjusted in the test. Then, floating fences were arranged in the towing tank, and artificial brash ice blocks were evenly added to the ice field. The test started with a small concentration, as shown in Fig. 6 (left). When the ship model passed through the ice field, the ice removal effect of the bow of the ship moved the brash ice to the sides of the hull, making the ice field uneven (Fig. 6 (right)). Therefore, the brash ice blocks in the ice field needed to be adjusted after each test to obtain an evenly distributed ice field. The next test could be conducted after the adjustment was completed and the water surface turned still.

The speed was controlled by a trailer in the towing tank. Speed tests at the four speeds of 0.3, 0.5, 0.7, and 0.9 m/s were carried out, and each working condition was repeated at least three times.

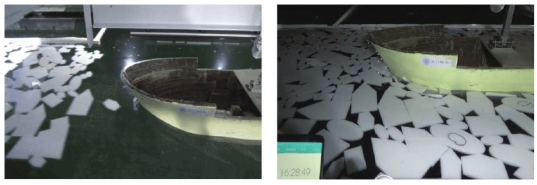

Fig. 6 Ship model entering the ice field (left) and its interaction with ice blocks when sailing in ice field (right)

2 Analysis and discussion of test results

2.1 Observations

Fig. 7 presents the time-history curve of resistance measured in a test run. The most salient feature of this curve is violent oscillations, while the time-history curve of open-water resistance is a smooth straight line. Clearly, the two curves are essentially different from each other. The oscillations of the resistance curve arise from the short-time collision between the brash ice and the hull. Consequently, the resistance curve has a time-history feature similar to that in the case of a periodic impact load. The comparison with the video reveals that after the collision, the brash ice blocks undergo the following motion situations:

1) They translate and rotate on the water surface, as shown in Fig. 8(a);

2) They flip on the vertical plane, as shown in Fig. 8(b);

3) They stick to the bow of the ship for a certain distance after they flip, as shown in Fig. 8(c);

4) They accumulate at the bow and sides of the ship, as shown in Fig. 8(d). As the hull-fitting is essentially the prolonged flipping of the brash ice blocks, the three motion modes in Figs. 8(a)−8(c) are actually the rigid motion of brash ice blocks in a three-dimensional space. Therefore, they can be classified into one category. This rigid motion comes from the normal collision between the hull and the brash ice blocks and basically does not involve the interaction among multiple brash ice blocks. The accumulation is more complicated and may occur before and after the collision. It is triggered by the interaction among the brash ice blocks after the collision between the hull and the brash ice blocks.

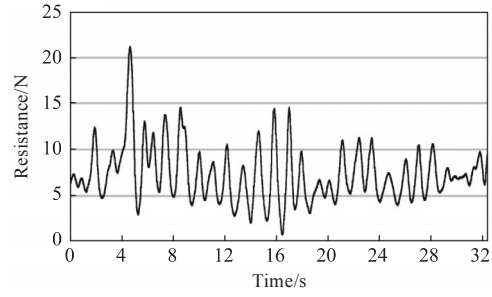

Fig. 7 Time-history curve of resistance measured in a test run

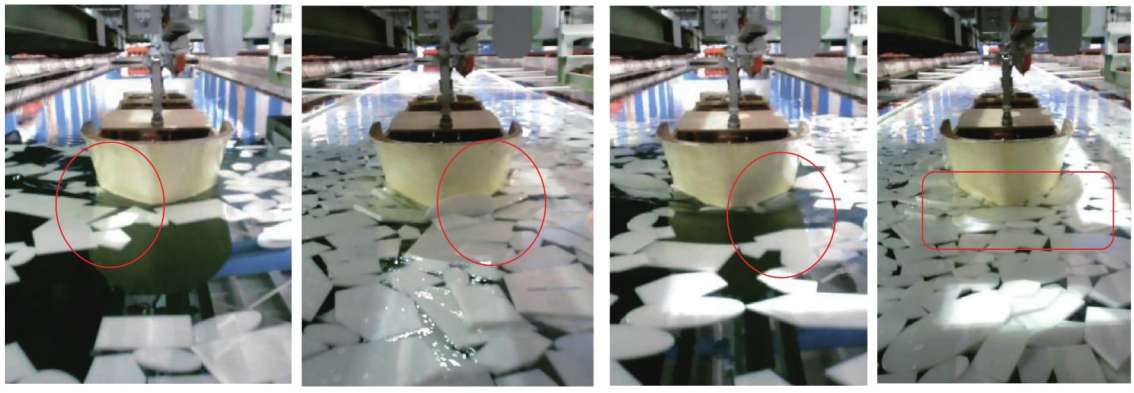

(a) Translation and rotation (b) Flipping (c) Hull-fitting (d) Accumulation

Fig. 8 Four types of motions of brash ice blocks observed in test after collision with hull

The resistance varies in different motion modes. Fig. 9 shows the time-history curve of resistance in 60−90 s when $\phi = 0.6$ and $U = 0.7$ m/s. The comparison with the video indicates that the 12 waves on the resistance curve in 60−77 s are caused by translation and rotation, while the seven waves in 77−90 s are induced by flipping. From the figure, the resistance in the case of flipping is generally much larger than that in translation and rotation.

Fig. 10 displays the comparison of resistance in the case of translation and rotation with that in accumulation, indicating that accumulation may also lead to violent oscillations of resistance.

The above four motion modes of brash ice blocks after collision do not occur with equal probability. Table 3 shows the frequency n of flipping during different test runs and its percentage in the total number N of ice blocks. It can be used to judge

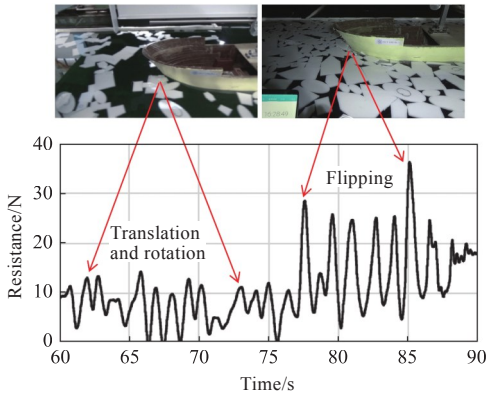

Fig. 9 Time-history curve of resistance in 60−90 s when ϕ = 0.6 and U = 0.7 m/s

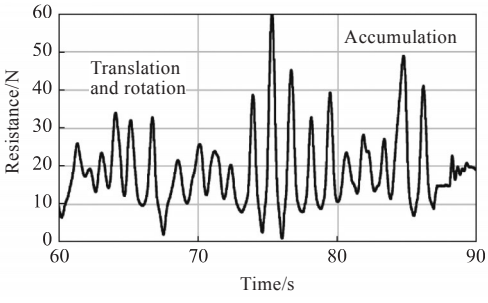

Fig. 10 High-amplitude oscillations in resistance produced by accumulation of brash ice blocks

which motion mode is more likely to occur under which circumstance. The frequencies of other motion modes can be obtained by analogy. Table 4 presents the most likely scenarios for the four modes to occur.

Table 3 Flipping frequencies of brash ice blocks under different speeds and concentrations

Speed and coverage	Test group	Total number N of ice blocks	Flipping frequency n	Flipping percentage /%	Acergae flipping percentage /%
U=0.3 m/s, ϕ=40%	01-1	825	11	1.33	1.12
	01-2	825	9	1.09	
	01-3	825	8	0.97	
	01-4	825	7	0.85	
	01-5	825	11	1.33	
U=0.9 m/s, ϕ=40%	04-1	825	43	5.21	8.06
	04-2	825	53	6.42	
	04-3	825	57	6.91	
U=0.3 m/s, ϕ=70%	13-1	1 440	148	10.28	8.37
	13-2	1 440	136	9.44	
	13-3	1 440	142	9.86	
U=0.9 m/s, ϕ=70%	16-1	1 440	153	10.63	11.39
	16-2	1 440	160	11.11	
	16-3	1 440	165	11.46	
	16-4	1 440	178	12.36	

Table 4 Likelihood of each phenomenon in different cases

	High concentration (60%, 70%)	Low concentration (40%, 50%)
Low speed(0.3 and 0.5 m/s)	Accumulation	Translation and rotation
High speed(0.7 and 0.9 m/s)	Flipping	Hull-fitting

2.2 Analysis of resistance

Resistance is random over time. Therefore, the test was divided into three stages: the initial stage, the stationary stage, and the end stage. A simple averaging method was adopted for analyzing the resistance in the stationary stage, with the results displayed in Fig. 11.

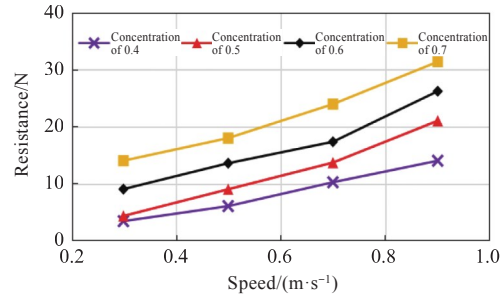

Fig. 11 Variation in average ice resistance (including open-water resistance) with speed under four concentrations

Total resistance R_T can be divided into two parts:

$$R_T = R_{OW} + R_I \tag{3}$$

where R_{OW} is open-water resistance; R_I is the ice resistance on the ship. Due to the low speed in this test, the wave-making resistance can be ignored. The open-water resistance mainly comes from the frictional water resistance. According to the ITTC-57 formula, open-water frictional resistance coefficient C_{OW} and open-water resistance R_{OW} are respectively

$$C_{OW} = \frac{0.075}{[\lg(Re)-2]^2}, \quad R_{OW} = \frac{1}{2}C_{OW}U^2S \tag{4}$$

where Re is Reynolds number; U is the speed; S is the wetted surface area.

The ice resistance R_I on the ship can be obtained by subtracting the open-water resistance R_{OW} from the total resistance R_T. The open-water resistance coefficient is defined by the square of speed U^2 and the wetted surface area S. However, the pure ice resistance coefficient cannot be defined by the two parameters. For one thing, the wetted surface area S should be replaced by the hull-ice contact area $A = Lh$, where L is the ship length. For another, the sizes of the brash ice blocks in the ice field are described by fractal dimension α that represents the probability of the contact between the hull and ice during the

ship motion and thus reflects the magnitude of resistance. Hence, the pure ice resistance coefficient C_I should be defined by U^α instead of U^2, and α is the fractal dimension in Eq. (2). Accordingly, the pure ice resistance coefficient was redefined as

$$C_I = \frac{R_I}{\frac{1}{2}\rho U^\alpha A}, \quad A = Lh \tag{5}$$

In the test, the pure ice resistance coefficient (minus open-water resistance) under the four concentrations is illustrated in Fig. 12. The figure tells that the laws of resistance coefficients are different in the discrete phase ($\phi < \phi_c$) and connected phase ($\phi > \phi_c$). In the test range (speed of 0.3−0.9 m/s), the ice resistance coefficient in the discrete phase hardly changes with the speed; it is merely a function of the concentration. In this case, ice resistance R_I, mainly caused by the collision of the brash ice blocks with the hull, is denoted as R_P. The corresponding resistance coefficient is the collision resistance coefficient, and it is expressed as follows:

$$C_P = \frac{R_P}{\frac{1}{2}\rho U^\alpha A} \tag{6}$$

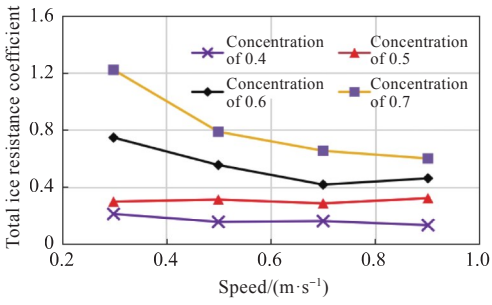

Fig. 12 Pure ice resistance coefficient under four concentrations

When $\phi > \phi_c$, the ice field becomes connected, as shown in Fig. 3(b). According to Table 4, accumulation occurs in this case, and a large frictional ice resistance is induced between the ice blocks and the hull. The frictional ice resistance R_μ is equal to the coefficient of kinetic friction μ multiplied by the normal force, and μ is related to normal pressure P. When P is changed under the same sliding speed, μ also changes, in a manner of decreasing with the increase in P[15-17]. In this case, the two objects slide against each other as a result of overcoming the engagement among the slightly convex parts because the surface of the objects is slightly convex rather than smooth. As the ice is of low hardness, the slightly convex parts in the actual contact area yield easily as the positive pressure rises. Consequently, ice surface roughness decreases, and the coefficient of kinetic friction declines accordingly. The variation in the coefficient of kinetic friction of ice with the normal pressure is expressed as $\mu \propto P^{-n}$. PP is harder than sea ice, and the gaps among PP piles are larger. Therefore, the coefficient of kinetic friction descends faster as the positive pressure grows. This paper assumed that this relationship still held, and n was determined according to the test. Due to the quadratic relationship between pressure and speed, namely, $P \propto U^2$, the coefficient of kinetic friction is $\mu \propto U^{-2n}$. Then, the frictional ice resistance can be expressed as

$$R_\mu \propto \mu PA = U^{2(1-n)}A \tag{7}$$

The corresponding frictional ice resistance coefficient is defined as

$$C_\mu = \frac{R_\mu}{\frac{1}{2}\rho U^\alpha A} \propto \frac{1}{U^{\alpha+2(n-1)}} \tag{8}$$

According to the above analysis, pure ice resistance can be decomposed into

$$R_I = \begin{cases} R_P, & \phi < \phi_c \\ R_P + R_\mu, & \phi \geqslant \phi_c \end{cases} \tag{9}$$

The resistance coefficient is

$$C_I = \begin{cases} C_P, & \phi < \phi_c \\ C_P + C_\mu, & \phi \geqslant \phi_c \end{cases} \tag{10}$$

According to the resistance data in Figs. 11−12 and Eqs. (6) − (10), resistance coefficient $C_I = C_P$ when $\phi < \phi_c$ can be estimated, as shown by the curves under concentrations of 0.4 and 0.5 in Fig. 13. When $\phi \geqslant \phi_c$, C_P and C_μ need to be estimated. C_P was obtained by simple fitting, as shown by the curves under concentrations of 0.6 and 0.7 in Fig. 13. Fig. 14 illustrates C_μ. When $\phi \geqslant \phi_c$, n was set to 1.5 in the calculation of the frictional resistance coefficient. The curves marked with "theory" in the figure were obtained from $C_\mu \propto \frac{1}{U^{2(n-1)+\alpha}}$, while those marked with "estimation" were obtained by subtracting the collision resistance coefficient from the data in Fig. 13.

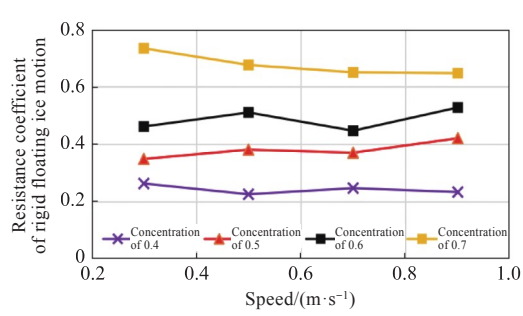

Fig. 13 Collision resistance coefficient

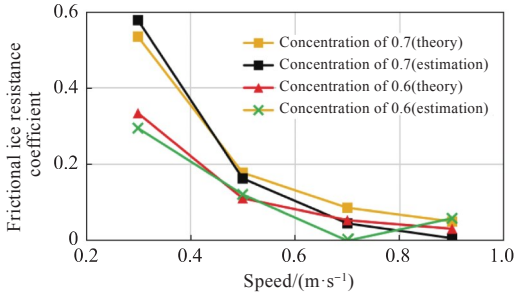

Fig. 14 Frictional ice resistance coefficient

The parameter n is set to −1.1 to −0.25 when the frictional resistance from actual sea ice is calculated [18]. The comparison with this paper reveals that the friction coefficient of artificial ice decays faster with speed than that of sea ice. It may be caused by the higher hardness of PP. Nevertheless, their variation laws are consistent.

3 Conclusions

Recent studies adopted substitute materials to investigate the resistance on ships in brash ice and achieved great progress, such as the verification of the feasibility and economy of substitutive artificial ice. In this paper, artificial brash ice made of PP was used to study the ice resistance on ships. The prediction method for brash ice resistance in the substitutive ice was obtained in the random ice field created in the towing tank, with the following results obtained:

When ϕ is between zero and one, the composition of ice resistance can be expressed as

$$R_{\mathrm{I}}=\begin{cases}R_{\mathrm{OW}}+R_{\mathrm{P}}, & 0<\phi<\phi_{\mathrm{c}}\\ R_{\mathrm{OW}}+R_{\mathrm{P}}+R_{\mu}, & \phi_{\mathrm{c}}\leqslant\phi<1\end{cases} \tag{11}$$

In the equation, the key is a critical concentration of $0.5<\phi_{\mathrm{c}}<0.6$ that determines the connectivity of the random ice field. When the concentration is smaller than the critical value, the main component of the resistance is the ice resistance caused by the collision of the brash ice blocks with the hull. When it is larger than the critical value, accumulation occurs in the ice field and produces a frictional ice resistance that decreases as the speed rises. In this case, the resistance consists of the ice resistance caused by the collision of brash ice blocks with the hull and the frictional resistance between the accumulated ice blocks and the hull. The scenarios in which frictional resistance and other resistance components occur were separated by introducing the critical concentration, and the dominant interval of each resistance component is presented.

Another important parameter is the fractal dimension α of the power-law distribution of brash ice blocks. U^{α} was used to define the resistance coefficient to keep C_{P} approximately equal to a constant, thereby facilitating test research.

To sum up, the ship model test using PP as artificial brash ice, instead of using natural frozen ice, is more economical and also provides a feasible alternative to the brash ice resistance test. However, the frictional resistance coefficient of PP declines faster with speed than that of natural frozen ice. Further research work is still needed to improve the model test.

References

[1] ZHU Y F, LIU Z Y, XIE D, et al. Advancements of the core fundamental technologies and strategies of China regarding the research and development on polar ships [J]. Bulletin of National Natural Science Foundation of China, 2015, 29(3): 178−186 (in Chinese).

[2] ZHANG C. China's "arctic silk road"[N/OL]. The Maritime Executive [2020-01-10]. https://maritime-executive.com/editorials/china-s-arctic-silk-road.

[3] REUTERS. Arctic sea route opens for the summer with first Yamal LNG cargo. The Moscow Times [N/OL]. [2019-07-05]. https://www.themoscowtimes.com/2019/07/05/arctic-sea-route-opens-for-the-summer-with-firstyamal-lng-cargo-a66306.

[4] BERGSMA J M, BOUHUYS C M, SCHAAP T, et al. On the measurement of submersion ice resistance of ships, using artificial ice [C]//Proceedings of the 24th International Ocean and Polar Engineering Conference (2014). Busan, Korea: ISOPE, 2014: 35−40.

[5] VAN DER WERFF S, BROUWER J, HAGESTEIJN J. Ship resistance validation using artificial ice [C]//Proceedings of the ASME 34th International Conference on Ocean, Offshore and Arctic Engineering (ISOPE 2015). St. John's, Newfoundland, Canada: ASME, 2015: V008T07A043.

[6] GUO C Y, XIE C, WANG S, et al. Resistance of ships in pack ice conditions [J]. Journal of Harbin Engineering University, 2016, 37(4): 481−486 (in Chinese).

[7] ZONG Z, YANG B Y, SUN Z, et al. Experimental study of ship resistance in artificial ice floes [J]. Cold Regions Science and Technology, 2020, 176: 103102.

[8] ZUEV V A, KALININA N V, MOSKVICHEVA Y A. Experimental studies of the resistance of transport ships at moving in composite broken ice [J]. IOP Conference Series: Materials Science and Engineering, 2021, 1079(7): 072016.

[9] FEDERS J. Fractals [M]. New York: Plenum Press, 1988: 104−148.

[10] STAUFFER D. Scaling theory of percolation clusters [J]. Physics Reports, 1979, 54(1): 1−74.

[11] KIM E, LU W J, LUBBAD R, et al. Toward a holistic load model for structures in broken ice [C]//The 23rd

International Conference on Port and Ocean Engineering under Arctic Conditions (POAC 15). Trondheim, Norway: [s.n.], 2015.

[12] TOYOTA T, TAKATSUJI S, NAKAYAMA M.Characteristics of sea ice floe size distribution in the seasonal ice zone [J]. Geophysical Research Letters, 2006, 33 (2): L02616.

[13] MANDELBROT B B. The fractal geometry of nature [M]. New York: W. H. Freeman & Company, 1982: 1−100.

[14] YU B M. Advances of fractal analysis of transport properties for porous media [J]. Advances in Mechanics, 2003, 33(3): 333−346 (in Chinese).

[15] SPENCER D, JONES S J. Model-scale/full-scale correlation in open water and ice for Canadian coast guard "R-class" icebreakers [J]. Journal of Ship Research, 2001, 45(4): 249−261.

[16] MAENO N, ARAKAWA M, YASUTOME A, et al. Ice-ice friction measurements, and water lubrication and adhesion-shear mechanisms[J]. Canadian Journal of Physics, 2003, 81(1−2):241−249.

[17] MAKKONEN L, TIKANMÄKI M. Modeling the friction of ice [J]. Cold Regions Science and Technology, 2014, 102: 84−93.

[18] WANG Q K. Study on the physical and mechanical engineering parameters of sea ice during melt season for arctic passage [D]. Dalian: Dalian University of Technology, 2018 (in Chinese).

碎冰阻力的替代试验及其变化规律研究

宗智[*1,2], 陈昭炀[1]

1 大连理工大学 船舶工程学院,辽宁 大连 116024

2 工业装备结构分析国家重点实验室,辽宁 大连 116024

摘　要:[**目的**]旨在探讨船舶碎冰阻力模型试验的替代方法及其变化规律,为冰区航行船舶的设计提供技术支持。[**方法**]使用聚丙烯材料替代天然的冻结冰,在常温拖曳水池中进行碎冰船模阻力试验。通过调整碎冰块的大小、形状、数量,可以产生给定密集度的随机碎冰场。根据几何相变理论,存在临界密集度,将碎冰冰场划分为离散相(密集度小于临界值)和连通相(密集度大于临界值)两种冰场。[**结果**]离散相冰阻力主要包括敞水阻力和碎冰块的船一冰碰撞阻力;连通相冰阻力成分除了敞水和碰撞阻力外,还包括堆积产生的冰摩擦阻力。采用基于随机冰场的分形维数来定义的阻力系数,发现当密集度小于临界值时,冰阻力系数在试验范围内(速度为0.3 ~ 0.9 m/s)近乎是常数;当密集度大于临界值时,冰摩擦阻力和速度呈反比。[**结论**]聚丙烯材料替代碎冰阻力试验具有可行性。碎冰场的纯冰阻力分为两个成分:碰撞产生的冰阻力和堆积产生的冰摩擦阻力。

关键词:碎冰;阻力;碰撞;摩擦